Available online at www.sciencedirect.com
SCIENCE DIRECT
Journal of Photochemistry and Photobiology A: Chemistry 176 (2005) 250–259
Journal of Photochemistry and Photobiology A:Chemistry
www.elsevier.com/locate/jphotochem

# Recent advances in the application of discharge-flow to the determination of gas-phase rate coefficients at pressures and temperatures of relevance to the Earth's atmosphere

Carl. J. Percival [a,*], Dudley E. Shallcross [b], Carlos E. Canosa-Mas [c], John M. Dyke [d]

[a] *School of Earth, Atmospheric and Environmental Sciences, The Sackville Building, The University of Manchester, Sackville Street, P.O. Box 88, Manchester M60 1QD, UK*
[b] *Biogeochemistry Research Centre, School of Chemistry, University of Bristol, Cantock's Close, Bristol BS8 1TS, UK*
[c] *Physical and Theoretical Chemistry Laboratory, University of Oxford, South Parks Road, Oxford OX1 3QZ, UK*
[d] *School of Chemistry, University of Southampton, Highfield, Southampton SO17 1BJ, UK*

Available online 24 October 2005

**Abstract**

The determination of gas-phase rate coefficients using the traditional discharge-flow system has produced a wealth of information that has informed atmospheric science. However, the range of pressure and temperatures observed in the Earth's atmosphere cannot be accessed by such a system. In this paper we discuss the recent advances in flow tube studies such as the use of turbulent flow that have allowed one to operate flow systems at atmospheric pressure and over a wider range of temperature. At the same time a number of new detection methods have been coupled to flow systems, such as CIMS, CEAS and UV-PES that have greatly enhanced the versatility and range of systems that may be studied and these are briefly discussed.


*Keywords:* Gas-phase kinetics; Discharge-flow; CIMS; CEAS; UV-PES

## 1. Introduction

The study of gas-phase chemical kinetics is of fundamental interest to physical chemistry. In particular, understanding the nature of radical–radical reactions, such as the factors controlling the pathways for atom recombination, the reactivity of excited states and their application to both combustion chemistry and atmospheric chemistry is of great contemporary interest. Recent advances in technology have facilitated the study of chemical kinetics to much lower temperatures (∼180 K) than previously accessible, using flash photolysis. Results from new low temperature kinetic studies have observed strong deviations from Arrhenius behaviour at low temperatures [1] as shown in the Arrhenius plot for the reaction of OH with acetone, Fig. 1. It is thought that the curved Arrhenius plot is a consequence of a change in mechanism. At lower temperatures a reactive channel that proceeds via the addition of OH to the carbonyl C atom followed by elimination of $CH_3$ from the energised adduct becomes accessible. Thus the simple extrapolation of higher temperature kinetic observations to temperatures that pertain to the Earth's atmosphere for example should only be undertaken with caution and may have considerable impact on atmospheric modelling studies. For, this reason research has focused on the development of experimental techniques that can experimentally access the temperatures and pressures that pertain to the Earth's atmosphere.

## 2. Experimental techniques

Traditionally, two types of technique have been used for the study of free radical reactions in the laboratory: in situ radical generation with real-time monitoring (flash photolysis) or separate radical generation and mixing in a laminar flow system, with detection as a function of contact time. The use of a laminar flow system has several advantages. Separate radical generation is much less susceptible to secondary chemistry than in situ generation, since radical sources do not interfere with each other. Also, the steady state conditions in a flow system readily permit signal accumulation. However, flow tubes have been limited

* Corresponding author. Tel.: +44 1612003945; fax: +44 1612003945.
*E-mail address:* carl.percival@manchester.ac.uk (Carl.J. Percival).

1010-6030/$ – see front matter © 2005 Elsevier B.V. All rights reserved.
doi:10.1016/j.jphotochem.2005.09.021

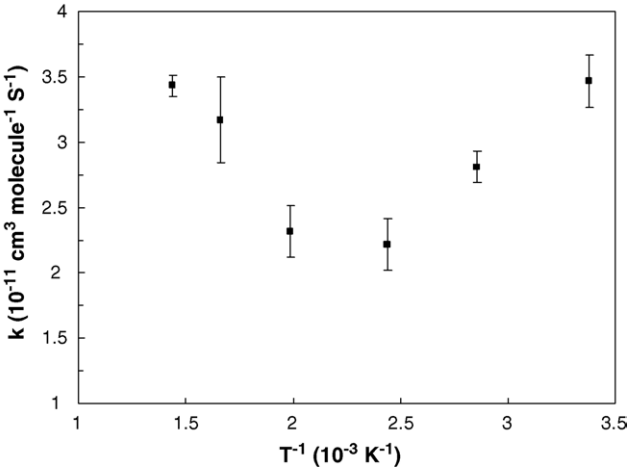


Fig. 1. Arrhenius plot for the reaction of OH with di-i-propoxymethane.

by the need to work at low pressures ($P$ = 1–20 Torr). There are inherent drawbacks to operating at such low pressures. First, the narrow pressure range severely hampers the study of termolecular reactions. Second, the collision frequency of trace species with the flow tube walls is very high, so that reactions at the walls interfere with measurements, particularly at low temperatures ($T$ < 250 K) [2]. As a consequence there is a lack of high quality kinetic data for radical–radical reactions below 250 K.

Operating under pseudo first order conditions and laminar flow it is assumed that the concentration of the limiting reagent, $C_a$, depends only upon the axial position and that the reactant transport in the axial direction is exclusively due to convection (i.e. axial diffusion is negligible). Under these assumptions the spatial variation of $C_a$ is given by the simplified continuity equation

$$-\bar{u} - \frac{dC_a}{dz} - k^I C_a = 0 \quad \text{(I)}$$

where $z$ is the axial position of reagent $C_a$, $k^I$ the pseudo first order rate coefficient for the reactive loss of $C_a$ and $\bar{u}$is the bulk gas velocity. Inspection of Eq. (1) shows that the approximations made to derive the equation are the equivalent of stating that each molecule travels at a velocity $\bar{u}$; which is commonly called the plug flow approximation. The plug flow approximation is only accurate when axial diffusion and radial concentration gradients are negligible. Axial diffusion effects are significant below 3 Torr, but can easily be accounted for by adding an axial diffusion term into the continuity equation [2]. However, radial concentration gradients can not be accounted for easily and represent the major limiting factor for the use of laminar flow systems.

There are two main sources of radial concentration gradients in the laminar flow regime. First, radial concentration gradients are formed when the radial transport of $C_a$ is much slower than the rate of chemical removal. This confines the reactive molecules to their original radial positions. Reactants at the centre of the tube experience shorter reaction times than those at the walls as a consequence of the peaked laminar velocity profile. Subsequently, the degree of homogeneous chemical depletion becomes more pronounced near the flow tube walls. Radial concentration gradients become more pronounced with increasing pressure because the diffusive transport correspondingly decreases. It has been found that rate constants using the plug flow approximation are unreliable when the pressure is above 10 Torr [2]. Second, radial concentration gradients are also formed if heterogeneous reactions occur to an appreciable extent on the flow system walls. For many species the heterogeneous loss at the walls has been found to increase dramatically as the temperature decreases. Although the reactivity of walls can be reduced by the use of coatings, the heterogeneous loss becomes prohibitively large at temperatures below 250 K [2].

In order to evaluate kinetic parameters at higher pressures a more detailed version of the continuity equation that includes axial and radial diffusion terms

$$D_A\left(\frac{1}{a}\frac{\partial}{\partial r}a\frac{\partial C_a}{\partial r} + \frac{\partial^2 C_a}{\partial z^2}\right) - 2\bar{u}\left(1 - \frac{r^2}{a^2}\right)\frac{\partial C_a}{\partial z} - k^I C_a = 0 \quad \text{(II)}$$

where $D_A$ is the molecular diffusion coefficient of the limiting reagent and $r$ is the radial co-ordinate. Poirer and Carr [3], Ogren [4] and Keyser [5] have developed analyses for the solution of the continuity equation for operating a flow tube at pressures up to 100 Torr. Correction factors, ranging from 1 to 2, are applied to experimentally observed rate coefficients to take into account these radial concentration gradients. The major limitations of such approaches are that one requires an accurate knowledge of the diffusion coefficients, correction factors increase as the pressure or wall activity increases and all analyses assume that the laminar flow is fully developed which becomes increasingly difficult at high pressures.

More recently, Abbatt et al. [6] extended the work of Keyser [5] by constructing a high pressure flow tube with a large internal diameter with multiple radical detectors. With this method they have determined rate constants in both laminar and turbulent f1ow conditions at pressures ranging from 7 Torr to nearly 400 Torr. The flow tube reactor of Abbatt and co-workers enables the values of $\nu$ and $C_a$ to be experimentally determined as functions of radial and axial position. Rate constants are determined by using the values of $C_a$ and $\nu$ determined in the continuity equation and numerically solving for $k$. Abbatt et al. [6] showed that it was possible to produce a “wall less” flow reactor where radicals were effectively confined to the core of the carrier gas flow. Operating under such conditions the diffusion times of radicals from the core to the wall of the reactor is of the order of 1 s whereas the experiments cover, typically, reaction times of 0.1 s. This greatly enhances the operating temperatures over which reactions can be studied, as wall catalysed reactions can be minimised at low temperatures. Although this approach can generate accurate rate constants, with errors of 6% [7] the experimental simplicity of the conventional flow tube technique has been sacrificed. Furthermore, the approach of Donahue and Anderson has so far been limited to the study of OH, $HO_2$ and H atom reactions (see, e.g. [8–10]).

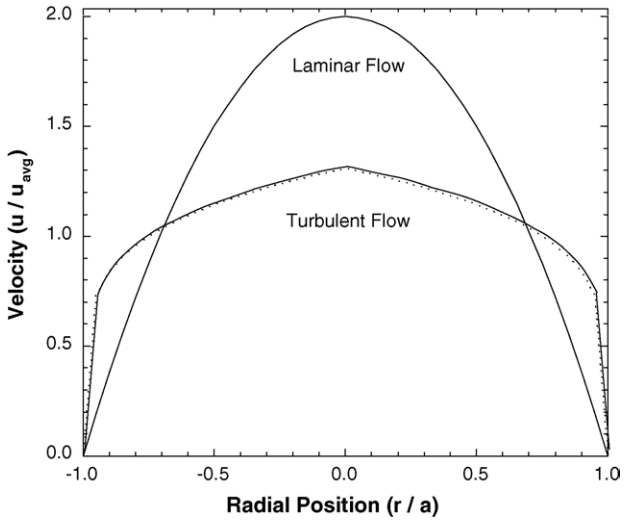


Fig. 2. Fully developed velocity profiles for the laminar and turbulent flow regimes.

### 2.1. Turbulent flow technique

Recently, a fast flow technique suitable for measuring elementary reactions over a wide range of pressures (60–760 Torr) has been developed [11–21]. Unlike the conventional flow technique, the method operates under turbulent flow conditions. Turbulent flow is achieved by operating under fluid flow conditions with Reynolds numbers greater than 3000

$$Re = \frac{2a\bar{u}\rho}{\mu} \quad \text{(III)}$$

where $Re$ is the Reynolds number, $a$ the internal radius of the flow tube, $\rho$ the density of the gas, $\mu$ the viscosity of the gas and $\bar{u}$is the bulk gas velocity. Fig. 2 shows a comparison of fully developed velocity profiles found in laminar and turbulent flow. It is readily seen in Fig. 2, that the turbulent flow velocity is flatter than the laminar flow profile. Therefore, working under turbulent flow conditions the plug flow approximation still holds and turbulent mixing by eddy diffusion allows the traditional versatility of flow tube methods to be regained when operating at higher pressures. Model simulations carried out by Seeley [22] indicate that operating in turbulent flow allows the plug flow approximation to be used at higher pressures with relatively little error (< 8%). The model assumes that turbulent flow is fully developed; reactants are mixed rapidly, with mixing distances <2$r$ and that the average velocity of the bulk gas can be used to define convective transport along the flow tube. Flow visualisation studies can be performed using the chemiluminescent reaction of oxygen atoms with nitric oxide. Fig. 3 shows flow visualisation results operating under turbulent flow conditions. As can be seen in Fig. 3a, using a simple open tube, reactants are not well mixed and "jet streaming" of the reactants occurs with mixing lengths much greater than 2$r$. However, if a turbulizer is placed on the end of the injector mixing occurs instantaneously on the time scale of the experiment, i.e. with mixing lengths of less than 2$r$, as shown in Fig. 3b. The addition of the turbulizer induces turbulence and promotes rapid mixing

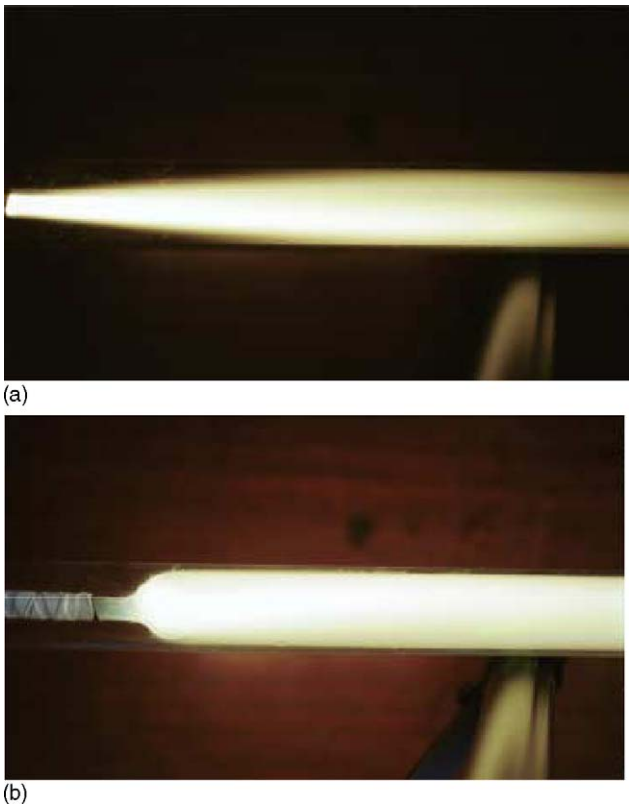


Fig. 3. A picture of mixing under turbulent flow conditions a, without a turbulizer and b, with a turbulizer placed at the sliding injector to induce turbulence.

of reactants. Indeed, experiments have shown that addition of a turbulizer can create fully developed turbulent flow along a flow tube at $Re < 3000$ [17].

Seeley et al. [11] have performed pulse trace studies to experimentally quantify deviations from plug flow conditions. Pulses of $Cl_2$ were added to the flow via a moveable injector and then $Cl_2$ was detected downstream via vacuum ultra violet fluorescence. The relative pulse velocity ($v$/vp; where $v$is the average bulk velocity and vp is the experimentally determined pulse arrival time) was evaluated by monitoring pulse arrival time as a function of contact time. Fig. 4 shows the relative pulse velocity as a function of $Re$. For $Re < 200$ the relative pulse velocity is unity, i.e. the plug flow approximation holds, For $Re > 200$ the relative pulse velocity increase, i.e. the plug flow approximation no longer holds. However, for $Re > 1000$ the relative pulse velocity decreases asymptotically with Reynolds number approaching unity.

Operating under turbulent flow conditions, Seeley et al. [11] estimated that deviations from the plug flow approximation result in apparent rate coefficients that are at most 8% below the actual values. Hence, flow corrections can be neglected, as they are smaller than the sum of other systematic experimental errors. Furthermore, the wall collision frequency for the reactants is greatly reduced in comparison with the conventional low pressure flow techniques which facilitates the study of gas phase kinetics at lower temperatures (180–300 K). Herndon et al. [23] and Chuong and Stevens [24] using different flow system configurations to that utilised by Molina and co-workers, have found

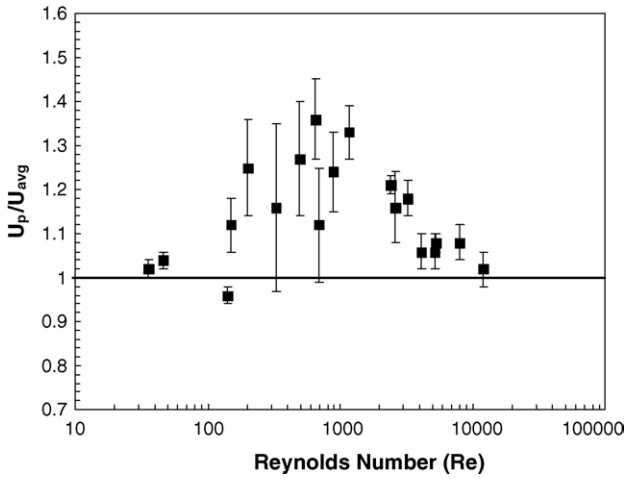


Fig. 4. A plot of the ratio of pulse arrival time:bulk velocity against Reynolds number.

the need to apply small corrections to the plug flow approximation in order to obtain accurate results using turbulent flow as a result of small deviations from the ideal conditions described by Seeley et al. [11]. However, the fact that no systematic errors have been apparent in the systems that have been studied to date with the flow configuration adopted by Molina and co-workers [19–21] no correction, in general, to the plug flow approximation is applied.

## 3. Chemical ionisation mass spectrometry

The extended temperature and pressure range of the turbulent flow system has been utilised by coupling to a chemical ionisation mass spectrometer (CIMS) for the study of the radical–radical reactions, as shown in Fig. 5. Unlike conventional electron impact mass spectrometers, CIMS produces ions at high pressures (20–760 Torr) via the formation of precursor ions. Precursor ions are formed via the action of either a corona discharge or a radioactive source, which then ionise the carrier gas. Operating in negative ion mode the secondary electrons, created from the ionisation of the carrier gas are captured via electron attachment, using for example $SF_6$, to produce the precursor ion. The precursor ion then reacts selectively with reagent

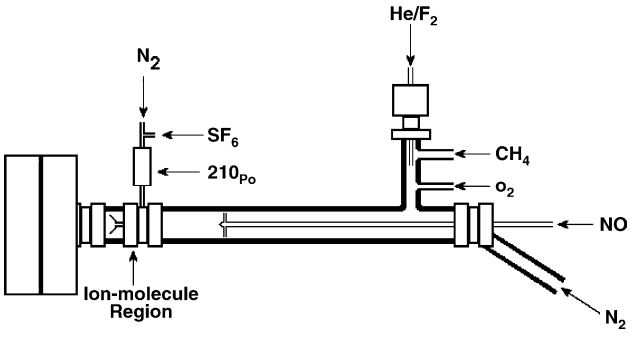


Fig. 5. A schematic diagram of the turbulent flow CIMS instrument for the study of $CH_3O_2$ + NO.

of interest, via a simple electron transfer reaction, for example

$$SF_6^- + NO_2 \rightarrow NO_2^- + SF_6 \quad (1)$$

$$SF_6^- + CF_3O_2 \rightarrow CF_3O_2^- + SF_6 \quad (2)$$

via fluoride ion transfer, for example

$$SF_6^- + HNO_3 \rightarrow NO_3{\cdot}HF^- + SF_5 \quad (3)$$

$$SF_6^- + HCl \rightarrow Cl \cdot HF^- + SF_5 \quad (4)$$

Or through a rearrangement reaction, for example

$$SF_6^- + HO_2 \rightarrow SF_4O_2^- + \text{products} \quad (5)$$

$$SF_6^- + CH_3O_2 \rightarrow FO_2^- + \text{products} \quad (6)$$

$CH_3O_2$ is detected as $FO_2^-$ (*m*/*e* 51). $FO_2^-$ signal only appears when F atoms, $CH_4$ and $O_2$ are present. The appearance of $FO_2^-$ signal as a function of reactant gases is shown in Fig. 6. Fig. 6 demonstrates that the $FO_2^-$ signal returns to background levels when either the $CH_4$, $O_2$ or $F_2$ flows are turned off. Hence $FO_2^-$ can only be attributed to the presence of $CH_3O_2$ radicals. A simple energetics analysis suggests that the reaction between $SF_6^-$ and $FO_2$ will produce highly energetic $FO_2^-$ ions and that these then have sufficient energy to decompose to $F^-$ and $O_2$. Although $FO_2$ radicals are being formed in the absence of $CH_4$ they cannot be detected as $FO_2^-$.

The use of different precursor ions enables the CIMS a wide variety of both radical and molecular species to be detected, e.g.

$$O_2^- + CF_3O_2 \rightarrow CF_3O_2^- + O_2 \quad (6)$$

$$NF_3^- + HO_2 \rightarrow HO_2^- + NF_3 \quad (7)$$

Table 1 summarises the species that have been detected using the CIMS technique for kinetic studies. The system can also be operated using positive ion–molecule chemistry; radical species have been detected via proton transfer, e.g. [25]

$$H_3O^+ + CH_3O_2 \rightarrow CH_3O_2H^+ + H_2O \quad (8)$$

$$H_3O^+ + C_2H_5ONO_2 \rightarrow C_2H_5ONO_2{\cdot}H^+ + H_2O \quad (9)$$

A further benefit of creating ions at high pressures is that ions can be focused by electrostatic lenses at each pumping stage and

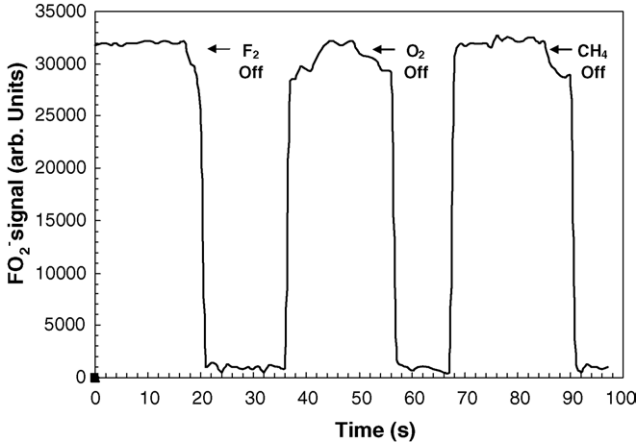


Fig. 6. $FO_2^-$ signal production.

Table 1
Observed chemical ionization pathways of a range of species detected for kinetic studies using various reagent ions[a]

| Precursor ion | Species | Ion detected | Reference |
|---|---|---|---|
| $F^-$ | $HO_2$ | PA | [13] |
| | $HO_2$ | $SF_4O_2^-$ | [13] |
| | $CH_3O_2$ | $FO_2^-$ | [18] |
| | $ClONO_2$ | CT | [15] |
| | ClO | CT | [15] |
| | OH | CT | [18] |
| | BrO | CT | [14] |
| | $NO_2$ | CT | [13] |
| | HCl | FT | [65] |
| | $HNO_3$ | FT | [65] |
| $SF_6^-$ | $Cl_2$ | CT | [65] |
| | $O_3$ | CT | [65] |
| | $C_7H_7O_2$ | CT | [66] |
| | $C_5H_8OHO_2$ | CT | [67] |
| | $CF_3O_2$ | CT | [68] |
| | $CF_3OH$ | FT | [68] |
| | $CF_3O$ | CT | [68] |
| | $CF_2O$ | $CF_3O^-$ | [68] |
| | $SO_3$ | FT | [69] |
| | $H_2SO_4$ | PA | [69] |
| | $CH_3O_2$ | CT | [70] |
| | $CH_3O_2$ | $CH_3^+$ | [70] |
| | $CH_3$ | CT | [70] |
| | $NO_2$ | CT | [70] |
| | NO | CT | [70] |
| $O_2^+$ | $C_7H_7O_2$ | CT | [66] |
| | $C_5H_8NO_3$ | CT | [71] |
| | $C_5H_8Cl$ | CT | [72] |
| | Oleic acid | CT | [73] |
| | Lineloic acid | CT | [73] |
| | 1-Ocatdecene | CT | [73] |
| | *n*-$C_3H_7O_2$ | CT | [74] |
| | *i*-$C_3H_7O_2$ | CT | [74] |
| | $C_2H_5O_2$ | CT | [74] |
| | Oleic acid | PA | [73] |
| $O_2^-$ | Lineloic acid | PA | [73] |
| | Octyl aldehyde | A | [73] |
| | Decyl alcohol | A | [73] |
| | Oleyl alcohol | A | [73] |
| $O_3^-$ | $NO_2$ | $NO_3^-$ | [75] |
| | $H_2SO_4$ | PA | [76] |
| $NO_3^-$ | $SO_3$ | CT | [76] |
| | $SO_3$ | A | [76] |
| $I^-$ | $N_2O_5$ | $NO_3^-$ | [77] |
| | $N_2O_5$ | A | [77] |
| $H_3O^+$ | $CH_3O_2$ | PT | [16] |
| | $CH_2O$ | PT | [16] |
| | $CH_3ONO_2$ | PT | [16] |
| | $C_2H_5O2$ | PT | [17] |
| | $C_2H_5O_2NO_2$ | PT | [17] |
| | $CH_3CHO$ | PT | [17] |
| | $C_3H_7O_2$ | PT | [25] |
| | $C_3H_7ONO_2$ | PT | [25] |
| | $CH_3C(O)C(O)CH_3$ | PT | [78] |
| | $CH_3C(O)CH_3$ | PT | [78] |
| | CH(O)CH(O) | PT | [78] |
| | $CH_3C(O)CH(O)$ | PT | [78] |
| | $CH_2(OH)CH_2O_2$ | PT | [79] |
| | $CH_3CH(OH)CH_2O_2$ | PT | [79] |
| | $CH_2(OH)CH(O_2)C_2H_5$ | PT | [79] |
| | $CH_3CH(OH)CH(O_2)CH_3$ | PT | [79] |
| | $CH_2(OH)C(O_2)(CH_3)_2$ | PT | [79] |
| | $CH_2(OH)CH(O_2)C_2H_3$ | PT | [79] |
| | $CH_2(OH)C(O_2)(CH_3)C_2H_3$ | PT | [79] |
| | $CH_2(Cl)CH_2O_2$ | PT | [80] |
| | $CH_2(Cl)CH(O_2)C_2H_5$ | PT | [80] |
| | $CH_3CH(Cl)CH(O_2)CH_3$ | PT | [80] |
| | $CH_2(Cl)C(O_2)(CH_3)_2$ | PT | [80] |
| | $CH_2(Cl)CH(O_2)C_2H_3$ | PT | [80] |
| | $CH_2(Cl)C(O_2)(CH_3)C_2H_3$ | PT | [80] |
| | Oleic acid | PT | [81] |
| | Nononal | PT | [81] |
| | 9-Oxononanoic acid | PT | [81] |
| | Azelaic acid | PT | [81] |
| | Nonanoic acid | PT | [81] |
| | Lineloic acid | PT | [73] |
| | Octyl aldehyde | PT | [73] |
| | 1-Ocatdecene | PT | [73] |
| | Oleyl alcohol | PT | [73] |
| $H_3O^+$ | Decyl alcohol | PT | [73] |
| | 2-Decanone | PT | [73] |
| $NO^+$ | Oleic acid | CT | [73] |
| | Lineloic acid | CT | [73] |
| | Octyl aldehyde | HA | [73] |
| | 1-Ocatdecene | PT | [73] |
| | Hexanal | A | [73] |
| | Oleyl alcohol | PT, A | [73] |
| | Decyl alcohol | PT | [73] |

[a] PT, proton transfer ($[M+H]^+$); CT, charge transfer ($M^+$ or $M^-$); A, association (e.g., $[M+NO]^+$); HA, hydride abstraction ($[M-H]^+$); PA, proton abstraction ($[M-H]^-$); FT fluoride ion transfer ($[M-F]^-$).

thus minimise loss of ion signal. It is assumed that the resultant ions are produced under pseudo first order conditions, i.e. at a fixed ion–molecule contact time and a fixed precursor ion concentration, the product ions produced are linearly proportional to the concentration of the species within the flow tube. Detector sensitivity is typically estimated from a linear plot of concentration versus ion signal, as shown in Fig. 7. CIMS is a highly

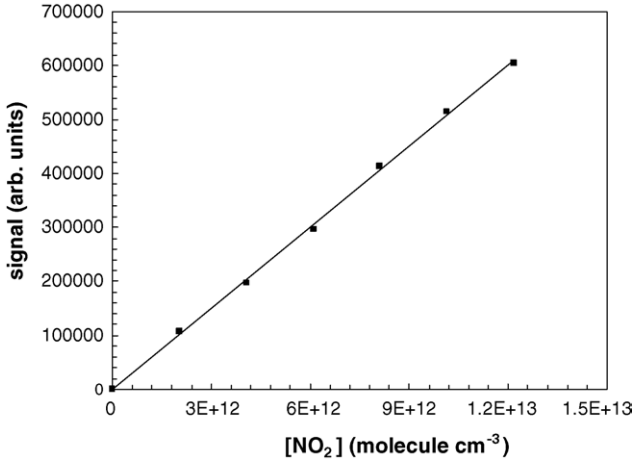


Fig. 7. A sensitivity plot for $NO_2$ (sensitivity is equal to one over the slope).

sensitive detector that has been used to monitor transient species in the laboratory at the ppt level.

The use of a turbulent flow-CIMS (TF-CIMS) enables radical reactions to be studied over a large range of pressures (70–760 Torr) and also facilitates the study of radical reactions at temperatures as low as 180 K. The highly sensitive CIMS detector allows kinetic studies to be undertaken at very low radical concentrations, typically (0.1–20) $\times 10^{10}$ molecule $cm^{-3}$. Such low radical concentrations ensures that numerical modelling is not required to deconvolute the rate coefficient from the observed concentration–time profiles. Furthermore, the versatility of the CIMS detector enables the quantification of products as a function of temperature and pressure, thus allowing the mass balance of reactions to be verified.

## 4. Other recent advances in detectors coupled with flow systems

### 4.1. Ultra-violet photo-electron spectroscopy

The use of electron impact mass spectrometry in gas kinetics to measure rate constants of simple atom–molecule or radical–molecule reactions is now well established. This method, which was developed by Clyne et al. [26–29] amongst others, involves molecular beam sampling from a flow tube and ionisation by impact with electrons in the energy region 30–70 eV. However, at these high electron impact energies fragmentation presents a severe problem and often the parent ion of one of the reagents is not observed. This problem becomes more severe as the reagents increase in size. However, the method has high detection sensitivity ($\approx 10^9$ molecules $cm^{-3}$) and has been used to measure rate constants for a large number of reactions [2].

In order to eliminate the problems of fragmentation and hence make the method more general, Dyke and co-workers have used photoionisation of reaction gases, sampled from a simple flow-tube system, energy analysed the photoelectrons and mass analysed the positive ions [30]. This combined use of UV-PES and PIMS can have a slightly reduced sensitivity ($\approx 10^{10}$–$10^{11}$ molecules $cm^{-3}$) compared with electron impact mass spectrometry but has a number of advantages. First, the photoelectron spectrum is not affected by fragmentation problems, it contains contributions from all species in the reaction mixture and one is able to distinguish between ground and excited states. Secondly, although PIMS spectra obtained, for example, at a photon energy of 21.22 eV still suffer from some fragmentation problems, a photoelectron spectrum recorded on the same gas sample as the PIMS spectrum, can be used to establish the parent peaks in the PIMS spectrum.

One of the major drawbacks with kinetic studies of gas-phase systems of interest to the atmosphere is the determination of products and their branching ratios. Although the discharge-flow technique can be coupled with mass spectrometry, product determination is particularly difficult for radical–radical reactions where multiple reaction pathways exist (e.g. [31]) and yet further complicated when dealing with isomeric radicals such as 1-$C_3H_7$ and 2-$C_3H_7$. Furthermore, excited states such as $O_2$ ($^1\Delta_g$) may well be important products from atmospherically important systems and indeed provide important information on reaction pathways. However, the UV-PES technique has potentially been able to address this problem for some time. Some examples of studies carried out in the last 20 years in the group of Dyke emphasise the versatility of the technique.

#### 4.1.1. $F + CH_3CH_2OH$ [32]

The experiment was carried out under high F atom concentrations and it was possible to observe as well as reagents, the reaction intermediates $CH_3CHOH$, $CH_3CHO$, $CH_3CO$, $CH_3$ and CF. Concentration time profiles were obtained for all species with CO and HF observed as the final products.

#### 4.1.2. $F + C_3H_8$ [33]

A range of primary and secondary reaction products were observed, but crucially, at short reaction times, both the 1-propyl and 2-propyl radicals were observed. The ratio of the two isomers produced, was in excellent agreement with literature values. The study emphasises the ability to detect isomeric radicals.

#### 4.1.3. $O + CH$ [34] and $O + CH_3C$ [35]

These chemiionisation reactions yielded $HCO^+$ and $CH_3CO^+$ as primary chemiions at the same time as chemielectrons. Secondary ions such as $H_3O^+$, $CH_3^+$, $C_2H_3^+$ and $C_3H_3^+$ were also observed. Similar studies have also been made for metal plus oxidant chemiionisation reactions [36].

#### 4.1.4. $Na + O_3$ [37]

In this study excited state NaO was observed as a product of the reaction between Na and $O_3$ using UV-PES. The ability to determine the yield of excited state products would be a major boost to atmospheric studies.

However, no quantitative studies of the rate coefficients had been attempted until very recently [38], where a conventional low pressure flow system was coupled with a UV-PES spectrometer to study the reaction between DMS ($CH_3SCH_3$) and molecular chlorine. It emerges that the reaction proceeds via a bound intermediate to yield molecular products HCl and $CH_3SCH_2Cl$ however, both the reactants, products and the intermediate could be observed during the course of the reaction. DMS is known to be a very important component of the climate system [39] and qualitative studies by Dyke and co-workers over the last decade [40–43] have shown that all key intermediates can be detected and quantified. Therefore, there is considerable promise in coupling UV-PES with conventional flow tube systems. Even though the sensitivity of the technique is poorer than conventional EI mass spectrometry, the range of species that can be detected suggests that it may go some way to allowing atmospheric scientists to tackle the problem of product determination.

### 4.2. Cavity enhanced spectroscopy

The use of a high-finesse cavity permits hundreds, or even thousands, of traverses through the absorber, and thus reaches markedly long effective path lengths and provides excellent

detection sensitivity. Cavity ring-down spectroscopy (CRDS), based on the measurement of the time for light to decay within the cavity [44–54]. The noise-equivalent absorption sensitivity is limited by the accuracy of the time-decay measurement, and reaches its optimum values with increasing reflectivity of the mirrors and an increasing optical base path length for each pass through the absorber and is typically in the range of $10^{-5}$ to $5 \times 10^{-9}$ [54,55] for a single pass through the cavity. The high sensitivity is achieved by arranging an isolation of the cavity from vibrations and by using external cavity laser diode, an optical isolator and an acousto-optic modulator. However, it is rather difficult to maintain isolation from vibration with the type of discharge-flow system used for gas phase kinetic measurements of reactive intermediates [56]. Extreme demands on the stability of the CRDS apparatus can therefore make these systems complex and expensive to implement.

The Wayne group, amongst others, e.g. [57–59], have developed a continuous wave (CW) cavity enhanced absorption spectroscopy (CEAS) with an off-axis alignment of the cavity geometry and with time integration of the output of the cavity for measurement of the absorption of narrow-band and broadband absorbers. The off-axis adjustment of the cavity can significantly reduce demands for optical isolation between the diode laser and the cavity, while detection of the time-integrated light of the cavity output can be performed by means of a low-frequency lock-in amplifier. This technique is significantly simpler than the other cw CRDS approaches based on fast digital signal-acquisition boards.

A typical experimental optical arrangement is shown in Fig. 8. The focused laser beam from a temperature controlled diode laser is directed through an interference filter into the absorption cell bounded by two plano-concave mirrors. Each mirror has its own holder mounted in adjustable gimbals. One of the mirror holders is fixed to a piezoelectric transducer (PZT) and a sinusoidal voltage ramp is applied to the PZT to provide modulation of the cavity length. A mechanical chopper is used to modulate the beam. The modulated light transmitted through the cavity is focused by a lens onto a photodiode that was coupled to an amplifier. The detected signal is then fed into a lock-in amplifier.

For the situation where there is no interference between a beam trapped in the cavity and an incident or output beam that overlap on the input or output mirror. For a cavity formed from two identical mirrors with intensity transmission and reflection coefficients $T$ and $R$, an overall output intensity $I_m$ after $m$ reflections can be written

$$I_m = c_g T^2 I_0 \, \mathrm{e}^{-(A_S+A_R+A_M)}(1 + R^2 \, \mathrm{e}^{-2(A_S+A_R+A_M)} + R^4 \, \mathrm{e}^{-4(A_S+A_R+A_M)} + \cdots + R^{2m} \, \mathrm{e}^{-2m(A_S+A_R+A_M)}) \quad \text{(IV)}$$

where $c_g$ is the coupling parameter, which is less than unity and depends upon the beam parameters and geometry of the cavity, $I_0$ the incident laser-beam intensity, $A_S$ the one pass loss due to the sample absorption, $A_R$ the one-pass loss due to molecular (Rayleigh) scattering and $A_M$ the one-pass loss due to particulate-matter (Mie) scattering. After simplification, (IV) can be written as

$$I_m = c_g T^2 I_0 \, \mathrm{e}^{-(A_S+A_R+A_M)} \times \left( \frac{1 - R^{2m+2} \, \mathrm{e}^{-(2m+2)(A_S+A_R+A_M)}}{1 - R^2 \, \mathrm{e}^{-2(A_S+A_R+A_M)}} \right) \quad \text{(V)}$$

where $A_S = [C]\sigma L_S$, $[C]$ is the concentration of the absorber, $\sigma$ the absorption cross section at the laser frequency and $L_S$ the single-pass absorption length, which can be as long as the cavity length $L$. After an arbitrarily large number of reflections in the stable cavity, the overall output intensity is given by

$$I = c_g T^2 I_0 \, \mathrm{e}^{-(A_S+A_R+A_M)} \frac{1}{1 - R^2 \, \mathrm{e}^{-2(A_S+A_R+A_M)}} \quad \text{(VI)}$$

For weak absorption ($A_S \ll 1$) and weak scattering ($A_R \ll 1$, $A_M \ll 1$), the relative change of the output intensity resulting from the presence of the absorber can be simplified to

$$\frac{I_N - I_S}{I_S} \approx \frac{A_S(1 + R^2)}{1 - R^2 + 2R^2(A_R + A_M)} \quad \text{(VII)}$$

where $I_N$ is the output intensity of the empty cavity and $I_S$ the output intensity with the absorber. For $(A_R + A_M) \ll (1 - R)$ and $R \approx 1$, the relative change of the output intensity is given by

$$\frac{I_N - I_S}{I_S} \approx \frac{A_S}{1 - R} = \frac{1}{1 - R}[C]\sigma L_S \quad \text{(VIII)}$$

Thus, for weak absorption, the cavity evidently provides an effective path length $L_S/(1 - R)$ and an absorption gain $G = 1/(1 - R)$, while the reflectivity of the mirrors can be derived from $R = (G - 1)/G$. Thus, for $(A_R + A_M) \ll (1 - R)$ and $R \approx 1$, the concentration of the absorber can be calculated from

$$[C] = \frac{I_N - I_S}{I_S} \frac{1 - R}{\sigma L_S} \quad \text{(IX)}$$

The minimum detectable concentration of absorbers will arise for maximum mirror reflectivity, maximum absorption cross section, maximum one-pass through the absorber and if the cavity-output intensity having no amplitude noise beyond its intrinsic quantum fluctuation. Under the shot-noise limit (shot noise predominates over thermal noise and background radiation) a ratio of the RMS intensity fluctuations ($\sigma_I$) to average intensity ($I_0$) incident on the photodiode is given as [60].

$$\frac{\sigma_I}{I_0} = \sqrt{\frac{-2e\Delta f}{\eta I_0}} \quad \text{(X)}$$

where $e$ is the electron charge, $\Delta f$ the bandwidth of the detection electronics and $\eta$ is the photodiode sensitivity. For instance, for a shot-noise limit, the value $\sigma_I/I_0$ can be as high as $1.3 \times 10^{-6}$ for a lock-in-amplifier time constant of 3 s (e.g. an equivalent noise bandwidth of 0.083 Hz at a filter slope of 6 dBoctave$^{-1}$) for an incident intensity of 100 nW and $\eta = 0.16$ AW−1 at $\lambda = 404$ nm. In practice, however, noise from various instrumental origins tends to become dominant and so can limit the detection sensitivity in off-axis CEAS.

Wayne and co-workers [61] developed the CEAS for the detection of the nitrate radical and have shown that the use

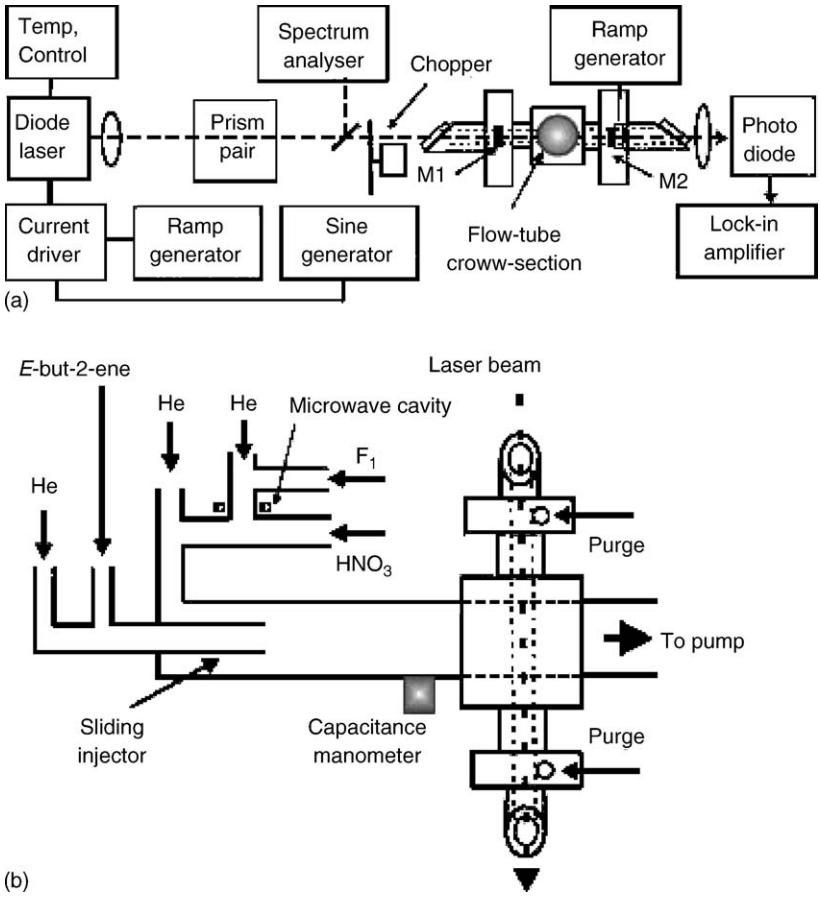


Fig. 8. (a) Experimental set-up for off-axis cw CEAS with cavity output intensity integrated over time. (b) Discharge-flow apparatus for the study of $NO_3$ with but-2-ene. Taken from Kasyutich et al. [61].

of the off-axis alignment of the cavity and simultaneous modulation of the cavity length and the diode laser wavelength allow minimisation of the intensity fluctuations induced by the cavity resonance, while preserving both the cavity amplification of the effective optical path through absorbers and the broadband optical-frequency transmission characteristic of the cavity. For the nitrate radical it has been shown that in this case, a noise-equivalent fractional absorption per one optical pass of $1.6 \times 10^{-6}$ was demonstrated at a detection bandwidth of 1 Hz, Which is the equivalent of noise-equivalent ($1\sigma \equiv$ root-mean-square variation of the signal) detection sensitivity of $5.5 \times 10^9$ molecule $cm^{-3}$. Thus the use of CEAS imparts orders of magnitude improvements in sensitivity in comparison to the use of both LIF and multipass White-cell absorption spectroscopy. Typically laser-induced fluorescence (LIF) detector [62] possesses a sensitivity of $\sim 10^{10}$ molecule $cm^{-3}$ (average of 300 measurements) towards $NO_3$ while a white cell utilising a tungsten–halogen lamp with an interference filter has a sensitivity towards $NO_3$ of $10^{11}$ molecule $cm^{-3}$ [63]. More recently Kasyutich et al. [61] have utilized CEAS for the detection of both $NO_2$ and IO and have achieved noise-equivalent detection sensitivities towards nitrogen dioxide of $1.8 \times 10^{10}$ molecule $cm^{-3}$ and towards the IO radical of $3.3 \times 10^9$ molecule $cm^{-3}$.

The use of a flow tube-CEAS (FT-CEAS) will facilitate the study of radical kinetics. The highly sensitive CEAS detector allows kinetic studies to be undertaken at low radical concentrations, typically $5 \times 10^{11}$ molecule $cm^{-3}$, i.e. under pseudo first order conditions. Indeed, Kasyutich et al. [61] studied the reaction of $NO_3$ with *E*-but-2-ene using FT-CEAS which yielded a rate constant of $(3.78 \pm 0.17) \times 10^{-13}$ $cm^3$ $molecule^{-1}$ $s^{-1}$ which is in excellent agreement with the recommended value of $(3.78 \pm 0.41) \times 10^{-13}$ $cm^3$ $molecule^{-1}$ $s^{-1}$. Furthermore the versatility of CEAS, via the use of a range of diodes, will enable the study of both the kinetic and mechanistic studies of a wide range of radical reactions, for instance, Bale et al. [64] have utilized FT-CEAS to study the reactions of peroxy radicals with iodine monoxide.

## 5. Conclusions

In 1979 Howard reviewed the determination of gas-phase rate coefficients by flow systems and listed a number of disadvantages, as well as many advantages. In the last 5–10 years, development of the turbulent flow reactor has breathed new life into flow tube studies, allowing a much wider range of pressures and temperatures to be accessed whilst still maintaining the versatility of the flow system in terms of radical prepara-

tion. At the same time a number of detection techniques, such as CIMS, CEAS and UV-PES, have been successfully coupled with flow systems and have provided routes to detecting a range of species that have hitherto been closed to flow tube interrogation. The future for flow tube approaches to determine gas-phase kinetic parameters is very bright.

## Acknowledgments

We are delighted to dedicate this paper to Professor Richard Wayne, a great friend and colleague and for CJP and DES a much valued D.Phil. supervisor. We wish him well in his retirement.

## References

[1] M. Wollenhaupt, S.A. Carl, A. Horowitz, J.N. Crowley, J. Phys. Chem. A 104 (2000) 2695.
[2] C.J. Howard, J. Phys. Chem. 83 (1979) 3.
[3] R.V. Poirier, R.W. Carr Jr., J. Phys Chem. 75 (1971) 1593.
[4] P.J. Ogren, J. Phys. Chem. 79 (1975) 1749.
[5] L.F. Keyser, J. Phys. Chem. 88 (1984) 4750.
[6] J.P.D. Abbatt, K.L. Demerjian, J.G. Anderson, J. Phys. Chem. 94 (1990) 4566.
[7] N.M. Donahue, J.S. Clarke, K.L. Demerjian, J.G. Anderson, J. Phys. Chem. 100 (1996) 5821.
[8] N.M. Donahue, M.K. Dubey, R. Mohrschladt, K.L. Demerjian, J.G. Anderson, J. Geophys. Res. 102 (1997) 6159.
[9] J.S. Clarke, J.H. Kroll, N.M. Donahue, J.G. Anderson, J. Phys. Chem. 102 (1998) 9847.
[10] J.S. Clarke, N.M. Donahue, J.H. Kroll, E. Uncu, H.A. Rypkema, J.G. Anderson, J. Phys. Chem. A 104 (2000) 5254.
[11] J.V. Seeley, J.T. Jayne, M.J. Molina, Int. J. Chem. Kinet. 25 (1993) 571.
[12] J.V. Seeley, J.T. Jayne, M.J. Molina, J. Phys. Chem. 100 (1996) 4019.
[13] J.V. Seeley, R.F. Meads, M.J. Elrod, M.J. Molina, J. Phys. Chem. 100 (1996) 4026.
[14] M.J. Elrod, R.F. Meads, J.B. Lipson, J.V. Seeley, M.J. Molina, J. Phys. Chem. 100 (1996) 5808.
[15] C.J. Percival, G.D. Smith, L.T. Molina, M.J. Molina, J. Phys. Chem. A 101 (1997) 8830.
[16] K.W. Scholtens, B.M. Messer, C.D. Cappa, M.J. Elrod, J. Phys. Chem. 103 (1999) 4378.
[17] D.L. Ranschaert, N.J. Schneider, M.J. Elrod, J. Phys. Chem. A 104 (2000) 5758.
[18] M.W. Bardwell, A. Bacak, M.T. Raventos, C.J. Percival, G. Sanchez-Reyna, D.E. Shallcross, Phys. Chem. Chem. Phys. 5 (2003) 2381.
[19] A.A. Miller, L.Y. Yeung, A.C. Kiep, M.J. Elrod, J. Phys. Chem. Chem. Phys. 6 (2004) 3402.
[20] A. Bacak, M.W. Bardwell, M.T. Raventos, C.J. Percival, G. Sanchez-Reyna, D.E. Shallcross, J. Phys. Chem. A 108 (2004) 10681.
[21] M.W. Bardwell, A. Bacak, M.T. Raventos, C.J. Percival, G. Sanchez-Reyna, D.E. Shallcross, Int. J. Chem. Kinet. 37 (2005) 253.
[22] J.V. Seeley, Experimental studies of gas phase reactions using the turbulent flow tube technique, Ph.D. Thesis, Massachusetts Institute of Technology, 1994.
[23] S.C. Herndon, P.W. Villalta, D.D. Nelson, J.T. Jayne, M.S. Zahniser, J. Phys. Chem. A 105 (2001) 1583.
[24] B. Chuong, P.S. Stevens, J. Geophys. Res. 107 (2002) 4162.
[25] J.M. Chow, A.M. Miller, M.J. Elrod, J. Phys. Chem. A 107 (2003) 3040.
[26] M.A.A. Clyne, R.T. Watson, J.C.S. Faraday I 70 (1971) 1169.
[27] M.A.A. Clyne, R.T. Watson, J.C.S. Faraday I 73 (1974) 1109.
[28] M.A.A. Clyne, A.J. MacRobert, Int. J. Chem. Kinet. 12 (1980) 79.
[29] M.A.A. Clyne, A.J. MacRobert, Int. J. Chem. Kinet. 13 (1981) 187.
[30] J.M. Dyke, N. Jonathan, A. Morris, Int. Rev. Phys. Chem. 2 (1982) 3.
[31] I.W.M. Smith, J. Chem. Soc. Faraday Trans. 87 (1991) 2271.
[32] J.M. Dyke, A.P. Groves, E.P.F. Lee, M.H. Zamanpour Niavaran, J. Phys. Chem. 101 (1997) 373.
[33] J.M. Dyke, A. Ellis, N. Jonathan, A. Morris, J. Chem. Soc. Faraday Trans. 2 (81) (1985) 1573.
[34] J.M. Dyke, A.M. Shaw, T.G. Wright, J. Phys. Chem. 99 (1995) 14207.
[35] J.M. Dyke, A.M. Shaw, T.G. Wright, J. Phys. Chem. 98 (1994) 6327.
[36] M.C.R. Cockett, L. Nyulaszi, T. Veszpremi, T.G. Wright, J.M. Dyke, J. Electron. Spectrosc. Relat. Phenom. 51 (1991) 373.
[37] T.G. Wright, A.M. Ellis, J.M. Dyke, J. Chem. Phys. 98 (1993) 2891.
[38] J.M. Dyke, M.V. Ghosh, D.J. Kinnison, G. Levita, A. Morris, D.E. Shallcross, Phys. Chem. Chem. Phys. 7 (2005) 866.
[39] R.J. Charlson, J.E. Lovelock, M.O. Andreae, S.G. Warren, Nature 326 (1987) 655.
[40] J. Baker, J.M. Dyke, Chem. Phys. Lett. 213 (1993) 257.
[41] J. Baker, J.M. Dyke, J. Phys. Chem. 98 (1994) 757.
[42] J. Baker, V.A. Butcher, J.M. Dyke, E.P.F. Lee, J. Phys. Chem. 99 (1995) 10147.
[43] J. Baker, J.M. Dyke, A.R. Ellis, A. Morris, J. Electron. Spectrom. Relat. Phenom. 73 (1995) 125.
[44] A. O'Keefe, D.A.G. Deacon, Rev. Sci. Instrum. 59 (1988) 2544.
[45] V.M. Baev, T. Latz, P.E. Toschek, Appl. Phys. B 69 (1999) 171.
[46] D. Romanini, A.A. Kachanov, N. Sadeghi, F. Stoeckel, Chem. Phys. Lett. 264 (1997) 316.
[47] K.J. Shulz, W.R. Simpson, Chem. Phys. Lett. 297 (1998) 523.
[48] J.B. Paul, L. Lapson, J.G. Anderson, Appl. Opt. 40 (2001) 4904.
[49] J.M. Herbelin, J.A. McKay, M.A. Kwok, R.H. Ueunten, D.S. Urevig, D.J. Spencer, D.J. Benard, Appl. Opt. 19 (1980) 144.
[50] R. Engeln, G. Helden, G. Berden, G. Meijer, Chem. Phys. Lett. 262 (1996) 105.
[51] R. Engeln, G. Berden, R. Peeters, G. Meijer, Rev. Sci. Instrum. 69 (1998) 3763.
[52] A. O'Keefe, Chem. Phys. Lett. 293 (1998) 331.
[53] A. O'Keefe, J.J. Shrerer, J.B. Paul, Chem. Phys. Lett. 307 (1999) 343.
[54] H.R. Barry, L. Corner, G. Hancock, R. Peverall, G.A.D. Ritchie, Chem. Phys. Lett. 333 (2001) 285.
[55] R.D. van Zee, J.T. Hodges, J.P. Looney, Appl. Opt. 38 (1999) 3951.
[56] A. Vipond, C.E. Canosa-Mas, M.L. Flugge, D.J. Gray, D.E. Shallcross, D. Shah, R.P. Wayne, Phys. Chem. Chem. Phys. 4 (2002) 3648.
[57] J.B. Paul, L. Lapson, J.G. Anderson, Appl. Opt. 40 (2001) 4904.
[58] D.S. Baer, J.B. Paul, M. Gupta, A. O'Keefe, Appl. Phys. B 75 (2002) 261.
[59] S. Williams, M. Gupta, T. Owano, D.S. Baer, A. O'Keefe, D.R. Yarkony, S. Matsika, Opt. Lett. 29 (2004) 1066.
[60] K.W. Bush, M.A. Bush (Eds.), Cavity Ring-down Spectroscopy: An Ultratrace-Absorption Measurement Technique, American Chemical Society Symposium, Ser. 720, Washington, DC, 1999.
[61] V.L. Kasyutich, C.E. Canosa-Mas, C. Pfrang, S. Vaughan, R.P. Wayne, Appl. Phys. B 75 (2002) 755.
[62] E. Martinez, B. Cabãnas, A. Aranda, R.P. Wayne, J. Chem. Soc. Faraday Trans. 92 (1996) 53.
[63] R.M. Chambers, A.C. Heard, R.P. Wayne, J. Phys. Chem. 96 (1992) 3321.
[64] C.S.E. Bale, C.E. Canosa-Mas, D.E. Shallcross, R.P. Wayne, Phys. Chem. Chem. Phys. 7 (2005) 2164.
[65] J.B. Lipson, T.W. Beiderhase, L.T. Molina, M.J. Molina, M. Olzmann, J. Phys. Chem. A 103 (1999) 6540.
[66] M.J. Molina, R. Zhang, K. Broekhuizen, W. Lei, R. Navarro, L.T. Molina, J. Am. Chem. Soc. 121 (1999) 10225.
[67] D. Zhang, R. Zhang, S.W. North, J. Phys. Chem. A 107 (2003) 11013.
[68] N.R. Jenson, D.R. Hanson, C.J. Howard, J. Phys. Chem. 98 (1994) 8574.
[69] J.T. Jayne, U. Poschl, Y. Chen, D. Dai, L.T. Molina, D.R. Worsnop, C.E. Kolb, M.J. Molina, J. Phys. Chem. A 101 (1997) 10000.
[70] P.W. Villalta, L.G. Huey, C.J. Howard, J. Phys. Chem. 99 (1995) 12829.
[71] I. Suh, W. Lei, R. Zhang, J. Phys. Chem. A 105 (2001) 6471.

[72] I. Suh, R. Zhang, J. Phys. Chem. A 104 (2000) 6590.
[73] J.D. Hearn, G.D. Smith, Anal. Chem. 76 (2004) 2820.
[74] J. Eberhard, C.J. Howard, Int. J. Chem. Kinet. 28 (1996) 731.
[75] G.D. Smith, L.T. Molina, M.J. Molina, J. Phys. Chem. A 104 (2000) 8916.
[76] T. Reiner, F. Arnold, J. Chem. Phys. 101 (1994) 7399.
[77] S.M. Kane, F. Caloz, M.T. Leu, J. Phys. Chem. A 105 (2001) 6465.
[78] L.Y. Yeung, M.J. Pennino, A.M. Miller, M.J. Elrod, J. Phys. Chem. A 109 (2005) 1879.
[79] A.M. Miller, L.Y. Yeung, A.C. Kiep, M.J. Elrod, Phys. Chem. Chem. Phys. 6 (2004) 3402.
[80] A.K. Patchen, M.J. Pennino, M.J. Elrod, J. Phys. Chem. A 109 (2005) 5865.
[81] J.D. Hearn, G.D. Smith, J. Phys. Chem. A 108 (2004) 10019.